

Modeling the sintering trajectories of MgAl2O4 spinel

Gabriel Kerbart, Christelle Harnois, Sylvain Marinel, Charles Manière

▶ **To cite this version:**

Gabriel Kerbart, Christelle Harnois, Sylvain Marinel, Charles Manière. Modeling the sintering trajectories of MgAl2O4 spinel. Scripta Materialia, 2021, 203, pp.114048. 10.1016/j.scriptamat.2021.114048 . hal-03403541

HAL Id: hal-03403541

https://cnrs.hal.science/hal-03403541

Submitted on 3 Nov 2021

HAL is a multi-disciplinary open access archive for the deposit and dissemination of scientific research documents, whether they are published or not. The documents may come from teaching and research institutions in France or abroad, or from public or private research centers.

L'archive ouverte pluridisciplinaire **HAL**, est destinée au dépôt et à la diffusion de documents scientifiques de niveau recherche, publiés ou non, émanant des établissements d'enseignement et de recherche français ou étrangers, des laboratoires publics ou privés.

Modeling the sintering trajectories of $MgAl_2O_4$ Spinel

Gabriel Kerbart[1], Christelle Harnois[1], Sylvain Marinel[1], Charles Manière[1*]

1 Normandie Univ, ENSICAEN, UNICAEN, CNRS, CRISMAT, 14000 Caen, France

Abstract

Controlling microstructure and density of $MgAl_2O_4$ spinel is a crucial step in the elaboration of industrial ceramics products. Understanding the sintering characteristics is a key issue to optimize the mechanical and optical properties. In this paper, Olevsky's sintering model is used to simulate the sintering trajectories of spinel. The densification and grain growth behaviors were identified via ramping and interrupted isothermal cycles highlighting the final stage sintering mechanisms change. The sintering trajectory model is intended to be a powerful numerical tool for sintering optimizations.

Keywords

Sintering; Sintering trajectory; Grain growth; Transparent Ceramics; $MgAl_2O_4$

The transparent spinel ceramic $MgAl_2O_4$ is an important material for a wide range of applications, such as jewelry, spacecraft windows, or protective transparent materials for military applications [1]. This interest is motivated by the excellent thermo-mechanical properties of spinel from room to high temperature (>1000°C), as well as its high hardness and fracture toughness, and the low cost of materials [2]. Furthermore, the spinel isotropic structure makes it very advantageous for the production of transparent ceramics thanks to the absence of birefringence. This material is consequently less sensitive to the optical transmission degradation due to the grain size effect.

Nevertheless, the properties of $MgAl_2O_4$ spinel are intrinsically linked to the microstructure of the material [3–5]. Controlling final stage sintering of spinel is therefore a key issue for ensuring optimal mechanical-optical properties. Numerous researches focus on the importance of the pre-sintering powder preparation [6,7] and on the influence of additives for reaching high densities [8–10]. The optimization of the sintering cycle is generally done by an experimental dilatometric study. The latter consists of trial and error methods to identify the right temperature and holding time to ensure full densification while retaining a small average grain size [11,12]. Two steps sintering strategies [13] are also investigated to achieve these objectives [14,15]. However, the experimental optimization of the sintering trajectory via the thermal cycle can be a time-consuming process. Indeed, each iteration step requires several hours of cycle, with long holding times, to reach interesting microstructures by free sintering [16–18]. The sintering trajectory modeling will therefore be of great interest for allowing an optimization study by computational approaches, after a previous experimental identification of the sintering model parameters. In this work, we will develop a comprehensive model to predict the sintering trajectory (evolution of grain size and densification) of $MgAl_2O_4$ spinel. Such a modeling is possible by a careful identification of the intermediate/final stage sintering behaviors and by the coupling of densification/grain growth models [19]. Similar approaches have been used for alumina [20], Zpex smile Tosoh zirconia [18], and also applied to

spark plasma sintering with a relevant model [21]. This model will take into account the transition of grain growth mechanism from surface diffusion for high porosity content, to lattice diffusion for low porosity, as previously shown for this material [22]. Furthermore, it will be shown that the final stage grain growth mechanism transition is accompanied by a densification behavior transition. These final stage phenomena will be compared to previous results obtained by a two-stages master sintering curve on the same material [23]. Finally, the sintering trajectory model will be compared to the experimental microstructural data for validation.

The densification/grain growth coupling has a great impact on the final stage sintering of ceramics. The sintering densification affected by grain growth has been formulated in Olevsky's model by the equation below [18]:

$$\dot{\theta} = \frac{-6\alpha(1-\theta)^3}{\frac{G^{m+1}}{G_0^m}\eta_0 T\psi exp(\frac{Q}{RT})} \quad (1)$$

With θ the porosity, $\dot{\theta}$ the porosity elimination rate (s^{-1}), T the absolute temperature, R the gas constant (J mol^{-1} K^{-1}), G and G_0 respectively the actual grain size and initial grain size (m), α the surface energy (J m^{-2}), η_0 the viscosity pre-exponential factor (Pa s), ψ the bulk modulus, Q the sintering activation energy (J mol^{-1}) and m the grain size exponent of the sintering behavior (m = 2 for lattice diffusion, and m = 3 for grain boundary diffusion [24]).

Assuming theoretical functions of ψ and the sintering stress [25,26], the linear regression of Equation (1) is used to determine the densification activation energy Q and the pre-exponential constant ratio $\frac{\eta_0}{\alpha}$ (Eq. 2)[27].

$$\frac{Q}{RT} + ln\left(\frac{\eta_0}{\alpha}\right) = ln\left(-\frac{6(1-\theta)^3}{\frac{G^{m+1}}{G_0^m}T\psi\dot{\theta}}\right) \quad (2)$$

In the sintering region where grain growth is inactive (initial and intermediate stages), the right term of equation (2) can be simplified as $\frac{G^{m+1}}{G_0^m} \sim G_0$. However, in this work, the grain growth parameters (see Equation (3) originated from ref[28]) are known as they were determined in our previous study ref[22].

$$\dot{G} = \frac{K_0 \exp\left(\frac{-Q_G}{RT}\right)}{G^p}\left(\frac{\theta_c}{\theta+\theta_c}\right)^n \quad (3)$$

θ_c and n are fitting constants required to adjust the porosity influence on the grain growth kinetics. K_0 is a pre-exponential factor, Q_G the grain growth activation energy and p the grain growth exponent (p=2 for pore control lattice diffusion and p=3 for pore control surface diffusion[24]).

Therefore, in the present study, the grain growth is considered in equation (2) right regression term (later noted Y). The latter is plotted *vs* 1/RT based on the dilatometry data and the grain growth model data.

Combining equations (1) and (3), the sintering trajectory can be modeled.

Samples are shaped by cold isostatic pressing (CIP) at 300 MPa of a commercial S30CR Baikowski spinel powder. This powder presents a specific surface area between 25 and 28 $m^2 g^{-1}$ (BET surface area), a material purity over 99 % and a d50 between 0.15 and 0.3 µm. The determination of the sintering behavior is based on dilatometry experiments (setsys 16/18, SETARAM), up to 1773 K, with three different heating ramps of 1, 2 and 5 K min^{-1} (Figure 1. a). Final relative density (RD_f) has been measured by Archimedes' method in ethanol and the actual relative density (RD_t) curve has been calculated from the specimen height (h_t) assuming isotropic shrinkage via $RD_t=RD_f h_f^3/h_t^3$ (see Figure 1. b). The corresponding dilatometry grain size evolution was determined from equation (3) (see Figure 1. c) and previously determined parameters (see appendix). With these data, the sintering parameters Q and $\frac{\eta_0}{\alpha}$ can be identified using equation (2) and assuming that densification is governed by the grain boundary diffusion mechanism (m=3). This first identification will be named "step 1". The activation energy from equation (2) direct method may be influenced by the ψ and Laplace stress porosity function from Skorohod's sintering theory [25,26]. This direct method is then compared with the master sintering curve (MSC) that has been done in a previous paper [23].

In order to explore the grain growth behaviors in isothermal regime, twelves interrupted experiments at 1673, 1773, 1873 K (Figure 1. d,e,f) were conducted in a previous study [22]. In this work, these data will be employed as final validation of the experimental/modeled sintering trajectories and for adjusting the model parameters. Latter validation step will be referred as "step 2".

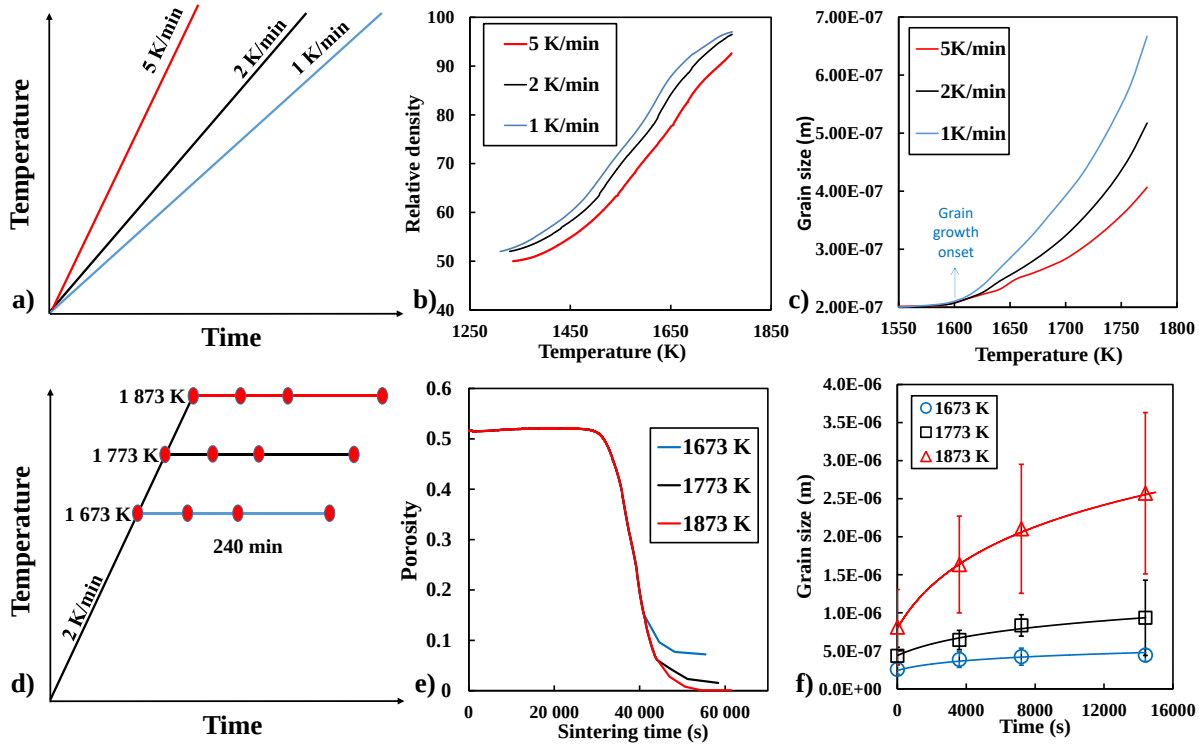


Figure 1 a) Heating ramp for dilatometry experiments, b) density during dilatometry experiments, c) grain size during dilatometry experiments, d) heating cycles used to determine the grain growth model (the red spots are the interruptions[22]), e) porosity evolution during sintering, f) grain size evolution with dwelling time.

The linear regression curves of the identification "step 1" are reported on Figure 2. Figure 2a points out two phenomena: first of all, a mismatch is observed between the curves corresponding to

the different heating rates, especially at low temperature, where the porosity is still important. This mismatch implies dissimilar intercepts, i.e. different pre-exponential viscosities (η_0). Secondly, whatever the heating rates, a change in the activation energy of densification appears systematically at the onset of grain growth (above 1600 K, see also figure 1c).

This regime transition could be understood by different phenomena such as, a regime change in defects formation at high temperature [29,30], the segregation of impurities at grain boundary, grain boundaries complexion[31,32] or a competition between the grain growth/densification diffusional mechanisms. In particular, we observed an exaggerated grain growth at to the specimen surfaces (see figure 2c and d) which seems to point out a high sensitivity to oxygen at high temperatures. In a previous study dedicated to MSC affected by grain growth [23], a similar difference in activation energy for sintering was observed from 400 kJ mol^{-1} below 1600 K to 700 kJ mol^{-1} above. In the literature, 750 kJ mol^{-1} were found for the same spinel powder grade formulated with a binder [33] and shaped by uniaxial pressing and CIP [34]; 530 kJ mol^{-1} was also reported by Tailimian *et al* [35] after milling of the same spinel grade. A similar transition regime was observed in an MSC study of zirconia[36].

Concerning the dissimilar densification behavior($\neq \eta_0$), one hypothesis to explain this difference may come from Skorohod [25,26] theoretical bulk modulus function $\psi = \frac{2}{3}\frac{(1-\theta)^3}{\theta}$. The latter modulus is based on an hypothesis which does not take into account the initial stage, where particle contacts imply a high sintering reactivity and a bulk modulus value close to zero [37]. The initial stage porous skeleton high reactivity can be considered by introducing a critical porosity θ_{cd} [38] inspired by Abouaf's moduli $\psi = \frac{2}{3}\frac{(\theta_{cd}-\theta)^3}{\theta}$ [39,40]. This critical porosity represents a porosity close to the green porosity leading the bulk modulus to tend towards zero. By adjusting θ_{cd} close to the green porosity, the bulk modulus has been corrected to obtain a unique densification sintering behavior (see figure 2b) accompanied by a flatter overall linearization. A θ_{cd} of 0.54 was obtained (a value close to the green porosity of 0.5).

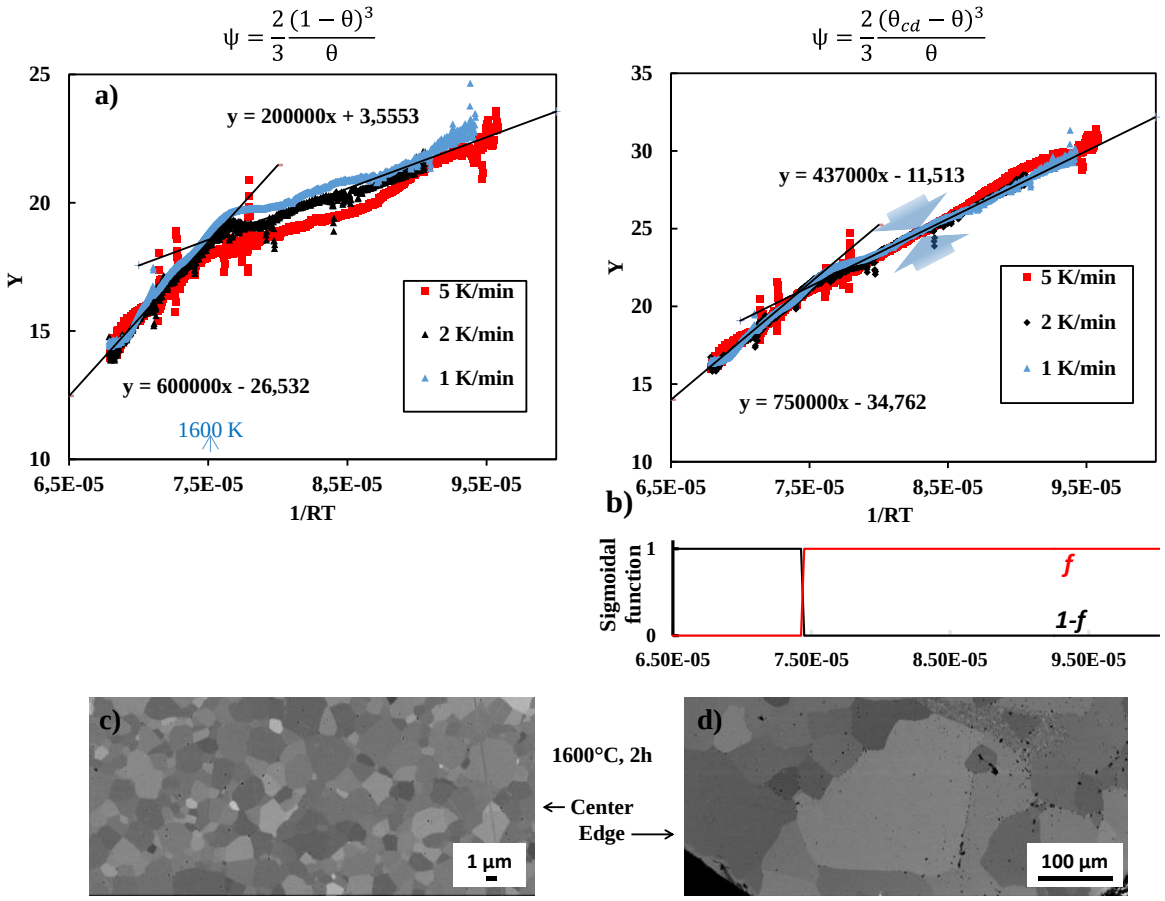


Figure 2 a) Determination of the sintering parameters without considering critical porosity, b) determination of the sintering parameters considering critical porosity, with below the corresponding sigmoidal functions used for the regime transition (c,d) center/edge microstructures at 1600°C showing the sensitivity of the microstructure close to the surface (air) at high temperatures.

To take into account the abrupt change of activation energy during sintering, a sigmoidal step function has been implemented in the model (see Appendix). We exposed on Fig.3 the validation (stage 2) of grain growth/densification modeling on isothermal tests. Two main comments can be made.

(i) We can see on Fig.3.a-b) that the model closely follows the experiments for both grain growth and density at lower temperature (1673 and 1773 K). However, there is a slight deviation at high temperature (1873 K). This deviation is imputable to the multiple changes in sintering energy activation and grain growth mechanisms at high temperatures. The important grain size difference between 1773-1873 K may be explained by the start of exaggerated grain growth as it was observed for spinel [4] and in figure 2c and d. We focus on the improvement of the model on the temperatures 1673 and 1773 K which are very important for the sintering optimization.

(ii) Concerning the sintering trajectory at 1673 K(Fig.3.c), the experimental points and the model exhibit higher grain sizes than the main trend of the other trajectory curves. This indicates that a holding at low temperature favors the coarsening rather than densification. The pore surface diffusion seems high for

this material against grain boundary diffusion. Consequently, low temperature holding should be avoided to reduce this coarsening zone.

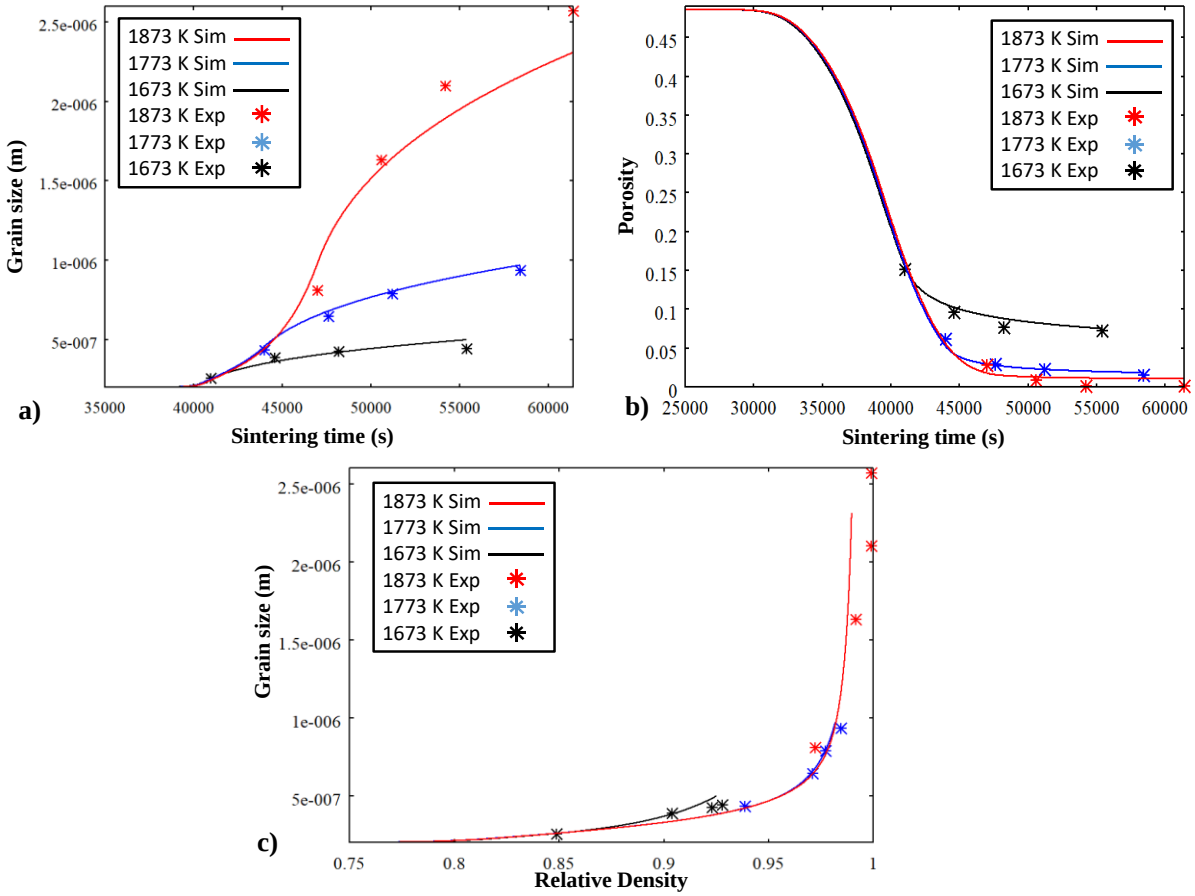


Figure 3 a) Grain growth modelisation results, b) sintering modelisation results, c) sintering trajectory modelisation results.

We have established a simple method in two steps for the identification of the sintering densification parameters of ceramics. This model (applied to $MgAl_2O_4$ spinel) reveals a regime transition of the densification parameters at the onset of grain growth. Furthermore, a dissimilar densification behavior has been highlighted especially before the onset of grain growth. However, we have shown that this apparent dissimilarity is caused by the bulk modulus function that should include the high sintering reactivity of the initial stage. Finally, the low temperature trajectories seem to indicate a highly active pore coarsening phenomenon. The latter may limit the densification if uncontrolled. Hence, sintering at this temperature (1673 K) should be avoided favoring thermal cycles like the two steps sintering where a rapid heating is employed to close the porosity with a minimum of coarsening. To conclude, we have determined the sintering parameters of $MgAl_2O_4$ spinel for both densification and grain growth, and we developed a predictive model for the sintering trajectory. This powerful numerical tool can be used to conduct sintering cycle optimizations for obtaining fine grained ceramics.

Appendix

The simulation of grain growth requires Olevsky's porosity function of the following form: $\left(\frac{\theta_c}{\theta+\theta_c}\right)^n$.

The values used in this model for θ_c and n are 0.001 and 0.25 respectively. Furthermore, the grain growth exponent was found to vary with the sintering temperature, as follows [22]:

$$p = 4.5.10^{-6}\,T^2 - 1.8207.10^{-2}\,T + 20.735 \quad (4)$$

The value used for the activation energy Q_G and K_0 are 1515kJ mol^{-1} and 6.014.10^{18} m s^{-1} respectively.

In order to take into account the low temperature (LT)/ high temperature (HT) jump in activation energy and pre-exponential factor, a sigmoidal function has been added in the code *via* the following form:

$$f = \frac{1}{1+exp^{-75(T-1619.31)}}. \quad (5)$$

Considering this function, the activation energy is expressed by:

$$Q = Q_{HT}*f + Q_{LT}*(1-f) \quad (6)$$

With Q_{HT}=750 kJ mol^{-1} and Q_{LT}=437 kJ mol^{-1}. Similarly, the pre-exponential term is expressed by:

$$\frac{\eta_0}{\alpha} = \left[\frac{\eta_0}{\alpha}\right]_{HT}*f+\left[\frac{\eta_0}{\alpha}\right]_{LT}*(1-f) \quad (7)$$

With $\left[\frac{\eta_0}{\alpha}\right]_{HT}$ = 8.10^{-16}Pa s m^{2}K^{-1}.J^{-1} and $\left[\frac{\eta_0}{\alpha}\right]_{LT}$ = 1.10^{-5}Pa s m^2 K^{-1} J^{-1}.

Acknowledgements

The authors thank Jérôme Lecourt and Christelle Bilot for their help in the progress of this study. We would like to thank the French ministery of research for PhD subvention of Gabriel Kerbart.

References

[1] S.F. Wang, J. Zhang, D.W. Luo, F. Gu, D.Y. Tang, Z.L. Dong, G.E.B. Tan, W.X. Que, T.S. Zhang, S. Li, L.B. Kong, Prog. Solid State Chem. 41 (2013) 20–54.

[2] J. Petit, L. Lallemant, in: B.J. Zelinski (Ed.), Conf. SPIE Def. + Secur., 2017, p. 101790K.

[3] J.A. Salem, J. Am. Ceram. Soc. 96 (2013) 281–289.

[4] M. Rubat du Merac, H.-J. Kleebe, M.M. Müller, I.E. Reimanis, J. Am. Ceram. Soc. 96 (2013) 3341–3365.

[5] M. Sokol, M. Halabi, Y. Mordekovitz, S. Kalabukhov, S. Hayun, N. Frage, Scr. Mater. 139 (2017) 159–161.

[6] D.-S. Kim, J.-H. Lee, R.J. Sung, S.W. Kim, H.S. Kim, J.S. Park, J. Eur. Ceram. Soc. 27 (2007) 3629–3632.

[7] C. Wang, Z. Zhao, Scr. Mater. 61 (2009) 193–196.

[8] N. Frage, S. Cohen, S. Meir, S. Kalabukhov, M.P. Dariel, J. Mater. Sci. 42 (2007) 3273–3275.

[9] S. Meir, S. Kalabukhov, N. Froumin, M.P. Dariel, N. Frage, J. Am. Ceram. Soc. 92 (2009) 358–364.

[10] M. Sokol, B. Ratzker, S. Kalabukhov, M.P. Dariel, E. Galun, N. Frage, Adv. Mater. 30 (2018) 1706283.

[11] L. Jiang, Y. Liao, Q. Wan, W. Li, J. Mater. Sci. Mater. Med. 22 (2011) 2429–2435.

[12] S. Marinel, C. Manière, A. Bilot, C. Bilot, C. Harnois, G. Riquet, F. Valdivieso, C. Meunier, C. Coureau, F. Barthélemy, Materials (Basel). 12 (2019) 2544.

[13] I.-W. Chen, X.-H. Wang, Nature 404 (2000) 168–171.

[14] J. Liu, X. Lv, J. Li, L. Jiang, J. Alloys Compd. 680 (2016) 133–138.

[15] J. Liu, X. Lü, J. Li, L. Hu, L. Jiang, Trans. Nonferrous Met. Soc. China 26 (2016) 2754–2761.
[16] J. Binner, K. Annapoorani, A. Paul, I. Santacruz, B. Vaidhyanathan, J. Eur. Ceram. Soc. 28 (2008) 973–977.
[17] S. Schwarz, O. Guillon, J. Eur. Ceram. Soc. 33 (2013) 637–641.
[18] C. Manière, G. Lee, J. McKittrick, S. Chan, E.A. Olevsky, Acta Mater. 188 (2020) 101–107.
[19] R.K. Bordia, S.-J.L. Kang, E.A. Olevsky, J. Am. Ceram. Soc. 100 (2017) 2314–2352.
[20] J. Zhao, M.P. Harmer, J. Am. Ceram. Soc. 75 (1992) 830–843.
[21] C. Manière, L. Durand, A. Weibel, C. Estournès, Ceram. Int. 42 (2016) 9274–9277.
[22] G. Kerbart, C. Manière, C. Harnois, S. Marinel, Appl. Mater. Today 20 (2020) 100759.
[23] G. Kerbart, C. Manière, C. Harnois, S. Marinel, J. Eur. Ceram. Soc. 41 (2021) 1048–1051.
[24] M.N. Rahaman, Sintering of Ceramics, CRC Press, 2007.
[25] V.V. Skorohod, Nauk. Dumka, Kiev (1972).
[26] E.A. Olevsky, Mater. Sci. Eng. R Reports 23 (1998) 41–100.
[27] C. Manière, E. Saccardo, G. Lee, J. McKittrick, A. Molinari, E.A. Olevsky, Results Phys. 11 (2018) 79–84.
[28] E.A. Olevsky, C. Garcia-Cardona, W.L. Bradbury, C.D. Haines, D.G. Martin, D. Kapoor, J. Am. Ceram. Soc. 95 (2012) 2414–2422.
[29] J.A. Ball, S.T. Murphy, R.W. Grimes, D. Bacorisen, R. Smith, B.P. Uberuaga, K.E. Sickafus, Solid State Sci. 10 (2008) 717–724.
[30] J.A. Ball, PhD, Computer Simulation of Disorder in Ceramic Materials, 2006.
[31] P.R. Cantwell, S. Ma, S.A. Bojarski, G.S. Rohrer, M.P. Harmer, Acta Mater. 106 (2016) 78–86.
[32] P.R. Cantwell, M. Tang, S.J. Dillon, J. Luo, G.S. Rohrer, M.P. Harmer, Acta Mater. 62 (2014) 1–48.
[33] N. Benameur, G. Bernard-Granger, A. Addad, S. Raffy, C. Guizard, J. Am. Ceram. Soc. 94 (2011) 1388–1396.
[34] E. Yamalaç, Sintering, Co-Sintering and Microstructure Control of Oxide Based Materials : Zirconia, Alumina, Spinel, Alumina-Zirconia and Spinel-Alumina, PhD, Genoble University and Izmir Institute of Technology, 2010.
[35] A. Talimian, V. Pouchly, H.F. El-Maghraby, K. Maca, D. Galusek, Ceram. Int. 45 (2019) 23467–23474.
[36] X. Song, J. Lu, T. Zhang, J. Ma, J. Am. Ceram. Soc. 94 (2011) 1053–1059.
[37] J.D. Hansen, R.P. Rusin, M.-H. Teng, D.L. Johnson, J. Am. Ceram. Soc. 75 (1992) 1129–1135.
[38] C. Manière, E.A. Olevsky, Scr. Mater. 141 (2017) 62–66.
[39] M. Abouaf, PhD, Modélisation de La Compaction de Poudres Métalliques Frittées, Approches Par La Mécanique Des Milieux Continus, Institut national polytechnique de Grenoble, 1985.
[40] M. Abouaf, J.L. Chenot, J. Theor. Appl. Mech. 5 (1986) 121–140.

Figures captions

Figure 1 a) Heating ramp for dilatometry experiments, b) density during dilatometry experiments, c) grain size during dilatometry experiments, d) heating cycles used to determine the grain growth model (the red spots are the interruptions[22]), e) porosity evolution during sintering, f) grain size evolution with dwelling time.

Figure 2 a) Determination of the sintering parameters without considering critical porosity, b) determination of the sintering parameters considering critical porosity, with below the corresponding sigmoidal functions used for the regime transition (c,d) center/edge microstructures at 1600°C showing the sensitivity of the microstructure close to the surface (air) at high temperatures.

Figure 3 a) Grain growth modelisation results, b) sintering modelisation results, c) sintering trajectory modelisation results.